JACS
JOURNAL OF THE AMERICAN CHEMICAL SOCIETY
Article
pubs.acs.org/JACS

Fabrication of $CaFe_2O_4$/TaON Heterojunction Photoanode for Photoelectrochemical Water Oxidation

Eun Sun Kim,[†] Naoyuki Nishimura,[‡] Ganesan Magesh,[†] Jae Young Kim,[†] Ji-Wook Jang,[†] Hwichan Jun,[†] Jun Kubota,[‡] Kazunari Domen,[‡] and Jae Sung Lee*[,†,§]

[†]Department of Chemical Engineering, Division of Advanced Nuclear Engineering, Pohang University of Science and Technology (POSTECH), 77 Cheongam-ro, Nam-gu, Pohang 790-784, Republic of Korea

[‡]Department of Chemical System Engineering, The University of Tokyo, 7-3-1 Hongo, Bunkyo-ku, Tokyo, Japan

[§]School of Nano-Bio Science and Chemical Engineering, Ulsan National Institute of Science and Technology (UNIST), 50 UNIST-gil, Ulsan, 689-798 Republic of Korea

Supporting Information

ABSTRACT: Tantalum oxynitride photoanode is fabricated and modified with calcium ferrite to form a heterojunction anode for a photoelectrochemical water splitting cell. The synthesized powders are loaded sequentially to the transparent conducting glass by electrophoretic deposition, which is advantageous to form a uniform layer and a junction structure. X-ray diffraction, UV−vis diffuse reflectance spectroscopy, scanning electron microscopy, and impedance spectroscopy analysis are conducted to investigate the structural, morphological, and electrochemical characteristics of the anode. The introduction of $CaFe_2O_4$ overlayer onto TaON electrode increases the photocurrent density about five times at 1.23 V vs reversible hydrogen electrode without any co-catalyst. Impedance spectroscopy analysis indicates that the junction formation increased photocurrent density by reducing the resistance to the transport of charge carriers and thereby enhancing the electron−hole separation. This photocurrent generation is a result of the overall water splitting as confirmed by evolution of hydrogen and oxygen in a stoichiometric ratio. From the study of different junction configurations, it is established that the intimate contact between TaON and $CaFe_2O_4$ is critical for enhanced performance of the heterojunction anode for photoelectrochemical water oxidation under simulated sun light.

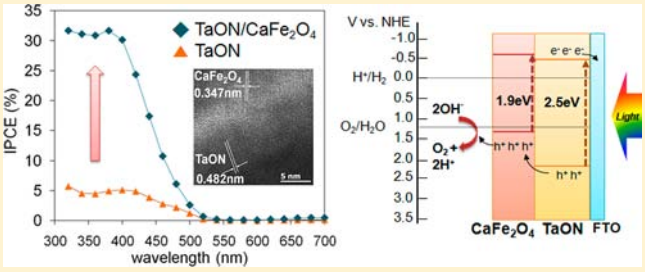

INTRODUCTION

Hydrogen is a promising alternative energy carrier of the next generation. When reacted with oxygen, hydrogen releases mechanical energy in engines or electric energy in fuel cells. It produces only water as a chemical product without any other pollutants including carbon dioxide. It also has a high-energy output per unit weight and can be transported and stored using established technologies. Among many paths for hydrogen production, the photoelectrochemical (PEC) cell is a highly promising system to produce hydrogen and oxygen from water using solar energy. Since the first concept was reported,[1] the semiconductor photocatalytic materials and fabrication techniques into photoelectrodes have been considered essential for high efficiency and have become the subjects of intensive research worldwide. For one thing, the absorption of a large fraction of visible light is required for photoanode material to achieve high efficiency in PEC cell under solar light irradiation. Most of researches are concentrated on simple metal oxides (Fe_2O_3,[2,3] WO_3[4,5] and $BiVO_4$[6−8]) because of their visible light activity, the stability in aqueous electrolyte, and low cost. More complicated binary and ternary oxides have also been investigated.[9−11] Recently, Domen and co-workers reported that oxynitride (TaON,[12,13] LaTiO2N[14]) and nitride (Ta_3N_5[15,16]) also showed stable and competitive performance as water oxidation photocatalysts.

In fabrication of the photoelectrode for PEC cells, prompt separation of photogenerated electrons and holes is extremely important to fully utilize the photoresponse of the material. The relationship between the long-lived photogenerated holes and the photocurrent was revealed in a recent report.[17] The p−n junction is the one of the design concept to separate electrons and holes by the internal electric field induced from band bending. The concept, originated from the design of high efficiency photovoltaic cells, has been successfully adopted for fabrication of semiconductor photocatalysts. However, because p-type semiconductor oxides are rather rare, the heterojunction photoanodes between two n-type semiconductors have been primarily studied, such as WO_3/$BiVO_4$[8,18] and Fe_2O_3/$ZnFe_2O_4$.[19]

Here we report results of the fabrication of a p−n heterojunction electrode between n-TaON and p-$CaFe_2O_4$.

Received: September 3, 2012
Published: March 6, 2013

   dx.doi.org/10.1021/ja308723w | J. Am. Chem. Soc. 2013, 135, 5375−5383

TaON was selected since it is highly active for water oxidation under visible light as particulate photocatalysts[20,21] as well as photoanodes of PEC cells[12,13] as reported by Domen and co-workers. It has a stable oxynitride phase, and its higher valence band maximum than the corresponding oxide is advantageous to have a smaller band gap energy. And $CaFe_2O_4$ is a p-type oxide semiconductor favored by Lee and co-workers to fabricate the p−n junction photocatalysts, such as $CaFe_2O_4$/$PbBi_2Nb_{1.9}W_{0.1}O_9$[22] and $CaFe_2O_4$/$MgFe_2O_4$.[23] Its valence band is more positive than water oxidation potential, and both conduction band and valence band are more negative than those of TaON.[24,25] Therefore these two semiconductors form staggered relative band positions as required to form an effective heterojunction photoanode.[26] $CaFe_2O_4$ was also applied as a single component photocathode for PEC cells,[27,28] yet its activity was extremely low.

Therefore, we fabricated a $CaFe_2O_4$/TaON p−n heterojunction photoanode for the first time and discovered that introduction of $CaFe_2O_4$ overlayer onto TaON electrode increased the photocurrent density about five times at 1.23 V vs reversible hydrogen electrode (RHE) without any co-catalyst. The origin of the remarkable activity enhancement was investigated.

EXPERIMENTAL SECTION

Synthesis of Photocatalyst Powder. Tantalum oxynitride was synthesized by heating tantalum oxide (Kojundo chemicals, 99.9%) under NH_3 gas flow (20 mL min^{-1}) at 850 °C for 15 h. Calcium ferrite was synthesized by a conventional solid-state reaction. A mixture of $CaCO_3$ (Wako Pure Chemicals, 99.99%) and Fe_2O_3 (Wako Pure Chemicals, 99.9%) was ground in an agate mortar in the presence of ethanol for 30 min and calcined at 1100 °C for 5 h.

Fabrication of Electrodes. The TaON electrode was prepared by electrophoretic deposition on F-doped SnO_2 glass (FTO, Asahi Glass) in a constant voltage mode following a previously reported procedure.[12] TaON powder (40 mg) was dispersed in acetone (50 mL) with iodine (10 mg, Sigma-Aldrich, ≥99.8%). The addition of iodine gave H^+ by the reaction with acetone and thus made particles positively charged. Two FTO glasses were immersed in the solution in parallel at a distance of 2 cm and 10 V of voltage was applied between the electrodes for 2 min using a dc power supply. The coated area was about 1 × 1 cm (denoted 'TaON-as deposited' electrode). The TaON-as deposited electrode was treated by a $TaCl_5$ solution for better connection between particles and electrode.[12] The 15 μL of $TaCl_5$ solution (Aldrich 99.8%, 10 mM in methanol) was dropped onto the electrode and dried. After repeating this process for five times, the electrode was heat treated in air at 400 °C for 30 min to obtain TaON-treated electrode. The $CaFe_2O_4$ layer was deposited on the TaON-treated electrode after the $TaCl_5$ solution treatment. The $CaFe_2O_4$ powder was dispersed in acetone with the same composition as used in TaON deposition. Electrophoretic deposition was conducted by applying 20 V bias for 1 min. The treatment with $TaCl_5$ solution also followed, and the electrodes were heat treated in air at 400 °C for 30 min to obtain TaON-treated/$CaFe_2O_4$ electrode. In addition, $CaFe_2O_4$ was deposited directly on the TaON-as deposited electrode, omitting the intermediate $TaCl_5$ solution treatment to obtain TaON-as deposited/$CaFe_2O_4$ electrode. The last electrode ensured direct contact between TaON and $CaFe_2O_4$ layers, and the $TaCl_5$ treatment was conducted in the final step only.

Characterizations. The obtained powders and fabricated films were characterized by X-ray diffractometer (M18XHF, MAC Science) with a monochromated Cu Kα radiation (λ = 1.54056 Å) at 40 kV and 200 mA. The UV−vis diffuse reflectance spectroscopy (UV−vis DRS) was used to probe the optical properties. The diffuse reflectance spectrum was obtained by a UV−vis recording spectrophotometer (UV-2401PC, Shimadzu) with an integrating sphere (ISR-240A, Shimadzu) and converted to the absorption spectrum by the Kubelka−Munk function.[29,30] The scanning electron microscopy (SEM) images and corresponding energy-dispersive X-ray spectroscopy (EDS) were obtained by FE-SEM (XL30S FEG, Philips Electron Optics). High-resolution transmission electron microscopy (HRTEM) was conducted with Image Cs-corrector (JEM-2200FS, JEOL). The focused ion beam (FIB, Helios, FEI) was used to prepare cross-sectional lamella of electrode.

X-ray photoelectron spectroscopy (XPS) analysis was used, and the spectra was obtained by ESCALAB 250 (VG-Scientific) spectrometer with X-ray source of Al Kα (hν = 1486.8 eV). The binding energy was calibrated using the C 1s peak at 284.6 eV.

Photoelectrochemical Measurements. The PEC cell test was conducted in a three electrode system with a potentiostat (Iviumstat, Ivium Technologies). The fabricated electrode, a platinum mesh, and Ag/AgCl electrode were used as working, counter, and reference electrodes, respectively. The cell was made of quartz glass, and 0.5 M sodium hydroxide at pH 13.7 was used as an electrolyte after saturation with nitrogen gas for 30 min. The 300 W Xe lamp (Xe Arc lamp source, model 66905, Oriel) equipped with a liquid IR filter (Water filter, model 61945, Oriel) and a cutoff filter (λ ≥ 420 nm, long pass filter, model 59840, Oriel) was used to irradiate only visible light. The photocurrent was measured by linear sweep voltammetry from −1.2 to 0.8 V (vs Ag/AgCl) with a scan rate of 0.01 V/s. The light irradiation came from the back side of FTO glass for all cases. For measurements of incident photon to current efficiency (IPCE), the 300 W Xe lamp was used with a liquid IR filter and a monochromator (Oriel Cornerstone 130 1/8 m monochromator) with a bandwidth of 5 nm. The cutoff filter (≥299 nm) was placed at the exit to prevent λ/2 radiation originated by Bragg diffraction at the grating. The incident light intensity was measured using a radiant power meter (model 70260, Oriel) with a photodiode detector (model 70282, Oriel). Potentiostatic electrochemical impedance spectroscopy (EIS) was carried out at a dc potential of 0.2 V vs Ag/AgCl with an ac potential frequency range from 100 000 to 0.1 Hz. The program ZView (Scribner Associates Inc.) was used to fit the obtained data to the corresponding equivalent circuit model.

Co-catalyst Loading and Gas Evolution Measurements. An oxygen evolving co-catalyst, cobalt phosphate (Co-Pi), was electrodeposited in a three electrode system by the method reported elsewhere.[31] The fabricated electrode, a platinum mesh, and Ag/AgCl were used as working, counter, and reference electrodes, respectively. The electrolyte solution was 0.5 mM cobalt nitrate hexahydrate in 0.1 M pH 7 potassium phosphate (KPi) buffer. The electrodeposition was conducted by applying 1.0 V vs Ag/AgCl for 2 min. After deposition of the co-catalyst, the electrodes were washed with distilled water and used to measure photocurrent. The electrolyte for photoelectrochemical cell was 0.1 M KPi buffered at pH 11.5 with 0.1 M KOH.

The hydrogen and oxygen evolution by photoelectrochemical water splitting was conducted in the airtight reactor connected to a closed gas circulation system. The 500W Hg lamp (Hg Arc lamp source, model 66902, Oriel) equipped with a liquid IR filter (Water filter, model 61945, Oriel) and a cutoff filter (λ ≥ 400 nm, long pass filter, model 59472, Oriel) was used to irradiate only visible light. The amount of hydrogen or oxygen was determined by a gas chromatography equipped with TCD (HP 6890, molecular sieve 5 Å column, Ar carrier gas).

RESULTS AND DISCUSSION

Physical Characterization of Photocatalysts and Photoanodes. The XRD pattern of the synthesized TaON powder is presented in Figure 1a.

It shows a monoclinic structure[32] (JCPDS no. 20-1235, space group = $P2_1/c$; a = 4.996, b = 5.034, c = 5.185 Å, β=99.65°) without any impurities such as Ta_2O_5 or Ta_3N_5. The XRD pattern of $CaFe_2O_4$ powder represents an orthorhombic structure[33] (JCPDS no. 32-0168, space group = *Pnam*; a = 9.228, b = 10.705, c = 3.018 Å) as shown in Figure 1b. The high noise of XRD patterns is a result of the fluorescence from the

dx.doi.org/10.1021/ja308723w | J. Am. Chem. Soc. 2013, 135, 5375−5383

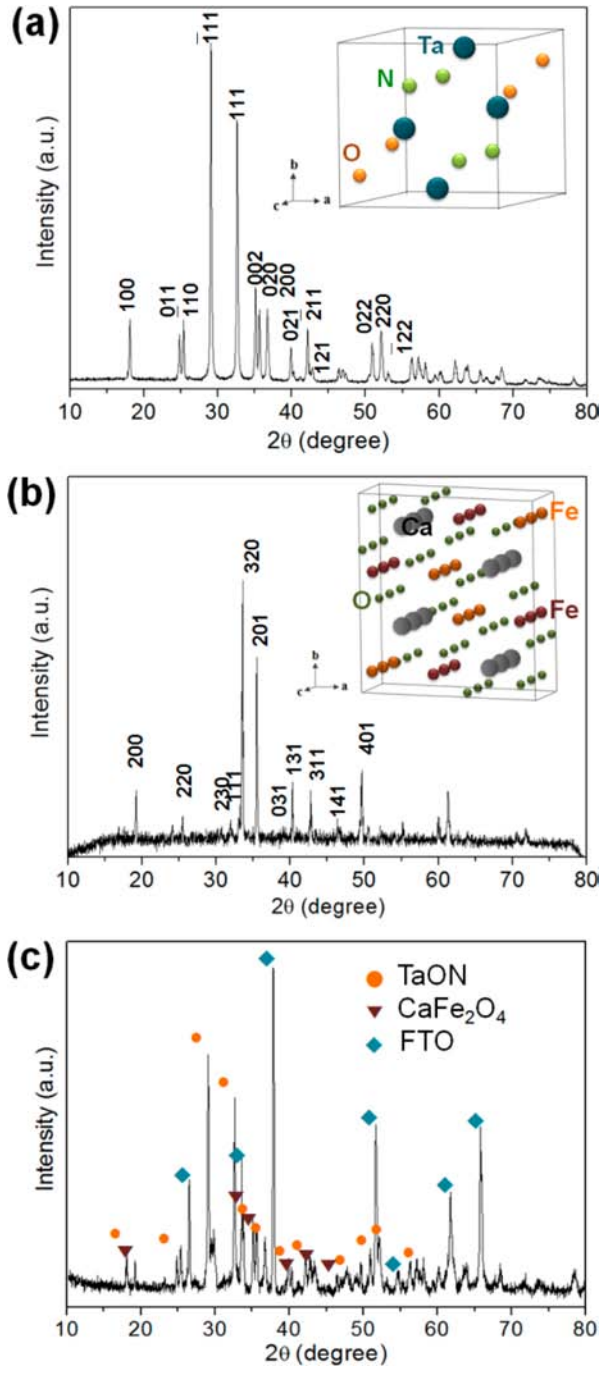

Figure 1. XRD pattern of (a) TaON (b) $CaFe_2O_4$ (c) TaON-as deposited/$CaFe_2O_4$ heterojunction electrode.

Fe atoms.[34] The TaON electrode fabricated by electrophoretic deposition with/without $TaCl_5$ treatment also showed similar pattern of TaON (Figure S1). The $TaCl_5$ treatment is known to help the connection between TaON particles, while preserving the original crystalline structure of TaON.[12,13] For TaON-as deposited/$CaFe_2O_4$ electrode, the intense peaks of TaON are dominant, and the weak peaks of $CaFe_2O_4$ are mixed as shown in Figure 1c. It can be concluded that $CaFe_2O_4$ layer was successfully deposited through the electrophoretic deposition.

The UV−vis DRS spectra of synthesized TaON and $CaFe_2O_4$ powders are shown in Figure 2. The UV−vis absorption of TaON has a clear edge around 500 nm, which

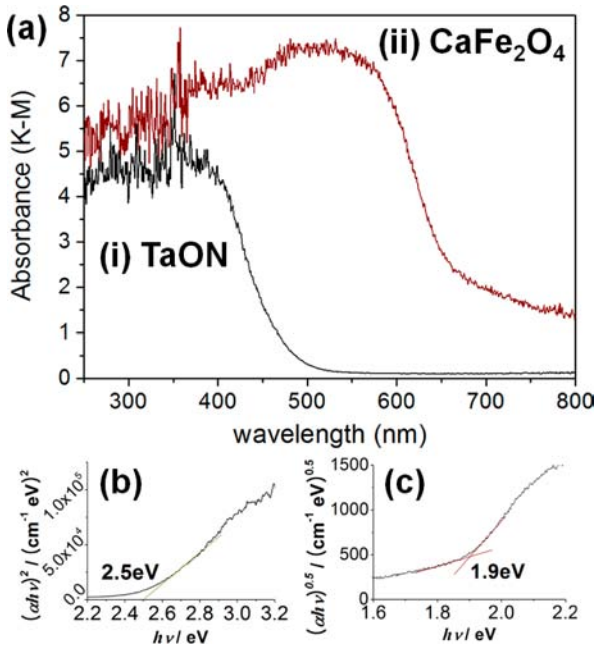

Figure 2. (a) UV-DRS of (i) TaON and (ii) $CaFe_2O_4$. The optical band gap was determined by Tauc plots shown for (b) TaON and (c) $CaFe_2O_4$.

corresponds to the band gap of TaON. The Tauc plot of TaON showed a direct optical band gap of 2.5 eV. The UV−vis absorption of $CaFe_2O_4$ shows an absorption edge around 650 nm which comes from the band gap of $CaFe_2O_4$. Its indirect optical band gap was determined to be 1.9 eV as shown in the Tauc plot. It also shows weak absorption in the extended region up to 800 nm as previously reported.[28] This absorption is common in ferrite material and comes from the trace of impurity energy levels.[24]

Morphological characteristics were investigated by SEM. At first, the SEM images of as-deposited TaON electrode showed uniformly deposited TaON layer of about 1−2 μm thickness with interparticle pores as presented in Figure 3a. The $TaCl_5$

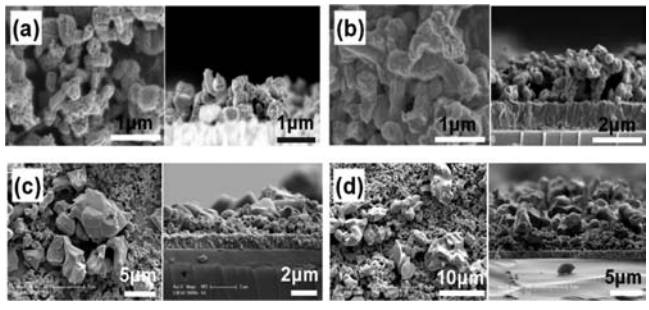

Figure 3. SEM images of electrodes (a) TaON-as deposited, (b) TaON-treated, (c) TaON-treated/$CaFe_2O_4$, and (d) TaON-as deposited/$CaFe_2O_4$. The left and right side images are top and side views for each electrode.

treatment clearly connected the TaON particles in TaON-treated electrode as shown in Figure 3b. From the side view of the TaON-treated electrode, the bottom of TaON layer still has porous structure even after the $TaCl_5$ treatment. It seems that the interparticle bridge formed by the $TaCl_5$ treatment does not block all surfaces of the film but gives porosity enough for facile penetration of electrolyte.

dx.doi.org/10.1021/ja308723w | J. Am. Chem. Soc. 2013, 135, 5375−5383

On top of the TaON electrodes, $CaFe_2O_4$ layer was deposited before and after the $TaCl_5$ treatment. The SEM images of the TaON-treated/$CaFe_2O_4$ electrode are shown in Figure 3c. The big particles are randomly dispersed like islands on top of TaON layer of smaller TaON particles rather uniformly with a thickness of about 2−3 μm. The big particles were also identified as $CaFe_2O_4$ with an atomic ratio of Ca:Fe = 1:2 by EDS analysis. The morphology of TaON-as deposited/$CaFe_2O_4$ in Figure 3d did not show significant difference as compared to TaON-treated/$CaFe_2O_4$, because the $TaCl_5$-treated layer between TaON and $CaFe_2O_4$ was hard to be seen by SEM images. The morphology of TaON-as deposited/$CaFe_2O_4$ electrode was investigated by HR-TEM as shown in Figure S2, which indicates the formation of a heterojunction between TaON and $CaFe_2O_4$. The smeared image of the interface shows that two materials make a close contact with no clear phase boundary line.

Photoelectrochemical Performance for Water Oxidation. The photocurrent density was obtained by applying potential in 0.5 M NaOH electrolyte under visible light irradiation (λ > 420 nm) as shown in Figure 4. The TaON-as

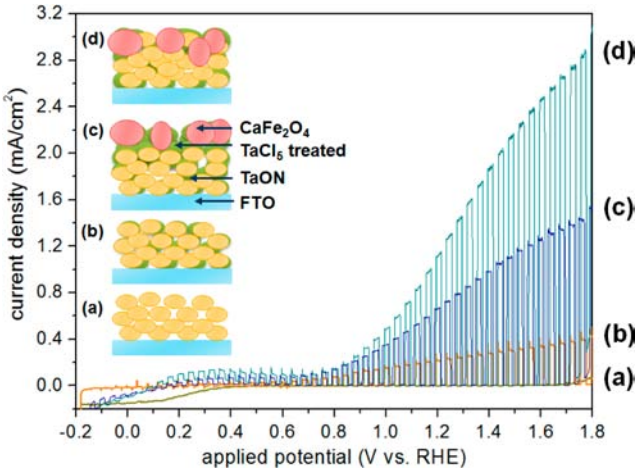

Figure 4. Photocurrent density of (a) TaON-as deposited, (b) TaON-treated, (c) TaON-treated/$CaFe_2O_4$, and (d) TaON-as deposited/$CaFe_2O_4$ in 0.5 M NaOH under chopped light irradiation (λ > 420 nm). Schematic models for four electrodes are also shown.

deposited electrode (Figure 4a) showed a negligible photocurrent density of about 4 μA cm^{-2} at 1.23 V vs RHE. The photocurrent density was read off at this potential hereafter, which is the standard reversible potential for water oxidation. The low current was attributed to the poor connection between particles and electrode as reported earlier.[12] The $TaCl_5$ treatment enhanced the connection by filling the void as shown in Figure 3b in the TaON-treated electrode. As a result, TaON-treated electrode (Figure 4b) showed greatly enhanced photocurrent of 0.23 mA cm^{-2}.

The duration of electrophoretic deposition (EPD) of TaON was optimized as 2 min at 10 V in the present study. The photocurrent was proportionally increased when EPD time increased from 1 to 2 min. The more TaON particles were collected on the FTO substrate under prolonged deposition time, and they rearranged themselves into a uniform film under the constant electric field. However, no further increase in photocurrent was detected when the deposition time increased from 2 to 3 min (not shown), indicating a saturation after ~2 min.[35] In this condition, TaON layer was uniformly deposited with the thickness of 1.5−2 μm as shown in the side view image of SEM (Figure 3b). Thus TaON deposition for all electrodes was conducted for 2 min hereafter.

Now on top of these TaON electrodes, $CaFe_2O_4$ layer was deposited by the same EPD with an optimized deposition time of 1 min (Figure S3). The TaON-treated/$CaFe_2O_4$ electrode (Figure 4c) showed a photocurrent density of 0.72 mA cm^{-2}. This represents an increase by a factor of >3 from that of TaON-treated electrode (0.23 mA cm^{-2}). At this point, we conjectured that the $TaCl_5$ treatment before the deposition of $CaFe_2O_4$ layer could hinder the direct contact between TaON and $CaFe_2O_4$ and thus desired junction formation. Therefore, TaON-as deposited was used as the base film, and $CaFe_2O_4$ layer was deposited with the $TaCl_5$ treatment delayed to the last step to obtain the TaON-as deposited/$CaFe_2O_4$ electrode. Indeed, this electrode showed the highest photocurrent of 1.26 mA cm^{-2} (Figure 4d), a factor of 5 enhancements as compared to the TaON-treated electrode. The result demonstrates that the contact between TaON and $CaFe_2O_4$ is critical to exhibit the full effect of heterojunction formation.

As a reference, a $CaFe_2O_4$ electrode was also fabricated by the same procedure, and the measured photocurrent response is shown in Figure S4a. The photocurrent was barely observed (<1 μA cm^{-2}) with the onset potential of 0.7 V (vs RHE). In addition to its intrinsic low activity,[27,28] the poor connection between the particles and the large particle size of $CaFe_2O_4$ (2−3 μm as shown in Figure 3c) may have contributed to the poor photoactivity. This extremely low photoactivity of $CaFe_2O_4$ itself makes the synergetic effect more impressive when it is paired with n-TaON forming a heterojunction. It is noteworthy that $CaFe_2O_4$ produces the anodic current, although this p-type semiconductor is known for water reduction activity and cathodic current generation.[27,28] The valence band edge (+1.27 V vs RHE) of $CaFe_2O_4$ is only slightly positive than water oxidation potential (+1.23 V vs RHE). But under this highly anodically biased condition, water oxidation seems possible on this material.

The scheme of cross sectional configurations for four electrodes shown in Figure 4 illustrates the structure and characteristics of each electrode. Tantalum oxynitride particles in TaON-as deposited electrode are deposited with large void between particles. The $TaCl_5$ treatment connects these particles together and particles to FTO substrate as in SEM images shown in Figure 3b. The Ta_2O_5 phase is formed between TaON particles upon $TaCl_5$ treatment and annealing in air.[12] However, its layer is relatively thin, and no significant peaks of Ta_2O_5 are detected in XRD pattern of TaON-treated electrode (Figure S1). The XPS analysis on TaON-treated electrode revealed the existence of Ta_2O_5 as discussed in Figures S5 and S6. This Ta_2O_5 layer could be converted into TaON by heat treatment in NH_3. There were some reports[12,13] that the heating of $TaCl_5$ treated electrodes in NH_3 flow improved photocurrent generation by forming additional TaON. But, in the present case, heating the TaON/$CaFe_2O_4$ electrode under NH_3 at 500 °C for 30 min decreased the photocurrent density of TaON-as deposited/$CaFe_2O_4$ and TaON-treated/$CaFe_2O_4$ decreased by 20% and 40%, respectively, after NH_3 treatment as shown in Figure S7. Thus, the NH_3 treatment at the high temperature appeared to have a detrimental effect on the $CaFe_2O_4$ layer, probably by creating defects in $CaFe_2O_4$ when nitrogen atoms replace a part of oxygen atoms. Hence, for all

dx.doi.org/10.1021/ja308723w | J. Am. Chem. Soc. 2013, 135, 5375−5383

cases of the $TaCl_5$ treatment, the NH_3 treatment was omitted, and the interfacial layer remained as Ta_2O_5.

During the electrophoretic deposition of $CaFe_2O_4$ onto TaON-treated or TaON-as deposited electrode, $CaFe_2O_4$ particles are drawn onto the substrate with a high throw power and fill the porous structure under applied electric field.[36,37] As a result, big $CaFe_2O_4$ particles can be partly imbedded into the pores of the formerly deposited TaON films. Thus the electrophoretic deposition is a facile and effective method to fabricate TaON and $CaFe_2O_4$ composite electrodes forming 3D junction structures extended over whole electrode areas. But the existences of $TaCl_5$ treated layer between TaON and $CaFe_2O_4$ cannot be distinguished by SEM image or XRD pattern as mentioned before. It may form a very thin layer coating of the particles. But their effect was obvious in the photocurrent generation performance of the films.

Charge Transfer in Photoanode Studied by EIS. Potentiostatic EIS was used to clarify the origin of the different photoelectrochemical responses of the different working electrodes as the photocurrent was generated under illumination of visible light. The impedance was measured at 0.2 V vs Ag/AgCl (1.23 V vs RHE), which was the same condition as the photocurrent measurements. The EIS results are presented in Figure 5a as Nyquist plots, where *x*- and *y*- axes are the real part (Z′) and the negative of imaginary part (-Z″) of impedance. Overall, the impedance of TaON-as deposited electrode was too large as compared to the other electrodes to show the all plots in the same scale. The enlarged part for TaON/$CaFe_2O_4$ electrodes is presented in Figure 5a. In general, a large value of impedance indicates a poor conductivity along the electron pathway in the electrode, yet the fitting of raw data to an equivalent circuit model is necessary for detailed analysis. Thus, the results were fitted into the models of two or three RC circuits (Figure 5b). The values of resistances (*R*) and constant phase elements (CPE) as a result of fitting are presented in Figure 5c. There are mainly two types of RC circuits in the system. The RC circuit with the largest resistance (R3/CPE3) usually represents electrode|| electrolyte interface,[38,39] and R1/CPE1 and R2/CPE2 are related to the electron transport inside the electrode.

The most remarkable in the EIS results is the drastic change in the third RC circuit (R3/CPE3) depending on electrodes. The resistance values (R3) decreased greatly in accordance with the increase of photocurrent generation in Figure 4. Since this circuit represents electrode||electrolyte interface, the decreased R3 indicates that the reactions by electron transfer at the surface should be more facilitated. It is the water oxidation reaction by the surface holes in this system, which is also responsible for the photocurrent generation. The resistance decreases when CPE increases from TaON-as deposited to TaON-treated, because the electrons at the surface of TaON-treated electrode could move faster than those on TaON-as deposited because of the connection between particles by the $TaCl_5$ treatment.

Consequently, water oxidation reaction could be accelerated and the photocurrent increased. Next, the charge transfer characteristics of TaON electrodes were dramatically improved by introduction of $CaFe_2O_4$ layer. The $CaFe_2O_4$ layer is expected to help the charge separation by forming a heterojunction with TaON. In addition, $CaFe_2O_4$ itself can also absorb photons and increase the density of charge carriers under illumination. Accordingly, the resistance decreased and capacitance increased as observed. This favorable effect was

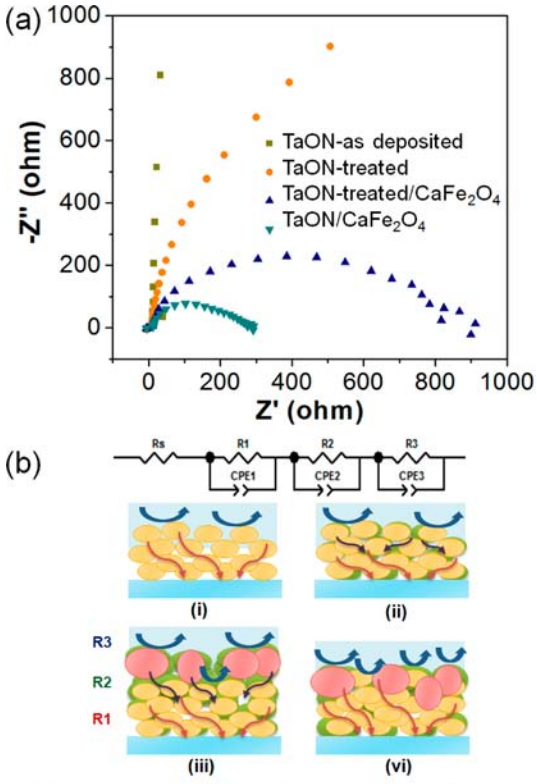

(c)

	Rs (Ω)	R1 (Ω) CPE1(μF)	R2 (Ω) CPE2(μF)	R3 (Ω) CPE3(μF)
(1) TaON-as deposited	9.05	46500 8.95		144000 11.5
(2) TaON-treated	9.44	993 9.37	1990 22.0	5720 74.9
(3) TaON-treated / $CaFe_2O_4$	9.99	149 8.86	324 20.7	334 150
(4) TaON-as deposited / $CaFe_2O_4$	10.8	121 6.21		152 206

Figure 5. (a) EIS of TaON/$CaFe_2O_4$ electrodes in Nyquist plots in 0.5 M NaOH under light irradiation (λ > 420 nm) at a dc potential of 0.2 V vs Ag/AgCl with an ac potential frequency range from 100 000 to 0.1 Hz. (b) Equivalent circuit model. Hole reactions on the surface and electron flow through the semiconductor film are noted. The connecting Ta_2O_5 layers are also indicated. (c) Resistance and CPE values of the corresponding models.

more pronounced for TaON-as deposited/$CaFe_2O_4$ because of the intimate TaON/$CaFe_2O_4$ contact without intervening Ta_2O_5 layers.

The first and second RC circuits represent the electron transport between particles and particles/FTO substrate at the electrodes. In TaON-as deposited electrode, there is only one circuit where electrons move through TaON particles. As presented in Figure 5c, the resistance on this way is too large because electrons have difficulty to pass through particle boundaries. The $TaCl_5$ treatment provides one more circuit in TaON-treated electrode by forming Ta_2O_5 between TaON particles. Although Ta_2O_5 is not active under visible light, the conduction band edge of Ta_2O_5 lies similar to that of TaON.[13] Thus electrons from TaON could move fast along Ta_2O_5 to another TaON particle (Figure S6). Hence, R2/CPE2 corresponds to the electron transport between particles either through grain boundaries or Ta_2O_5 bridges, and R1/CPE1 is the electron transfer from TaON particles to FTO substrate.

dx.doi.org/10.1021/ja308723w | J. Am. Chem. Soc. 2013, 135, 5375−5383

Compared to TaON-as deposited electrode, R1 was greatly decreased by the accelerated electron transport with $TaCl_5$ treatment. The Ta_2O_5 bridges can also exist at the bottom part of electrode contacting with FTO. But the value of CPE1 did not change significantly indicating that the $TaCl_5$ treatment did not bring the huge difference in the charge gradient here. In both cases, TaON faces FTO (TaON|FTO) and TaON and Ta_2O_5 have similar conduction band position as mentioned before.

When $CaFe_2O_4$ was brought onto TaON-treated, there are also two RC circuits, and the resistance decreased to a large extent. Because $CaFe_2O_4$ was deposited after $TaCl_5$ treatment, it could contact both with Ta_2O_5 phase and TaON particles. The electron and hole separation was facilitated by TaON/$CaFe_2O_4$ junction, which reduced the resistance on the movement of charge carriers. As a result, both R1 and R2 of TaON-treated/$CaFe_2O_4$ decreased. Only one circuit was observed again for TaON-as deposited/$CaFe_2O_4$. It suggests that the junction between TaON and $CaFe_2O_4$ is well formed facing each other as mentioned before. So there is one circuit presenting the electron movement between particle and electrode as in TaON-as deposited with the smallest R1 and R3 value by an effective heterojunction. As stated above, R1/CPE1 of TaON-as deposited/$CaFe_2O_4$ showed only a marginal change from that of TaON-treated/$CaFe_2O_4$ because of the similar configuration at the TaON|FTO interface.

Incident Photon to Current Efficiency (IPCE). The IPCE values (or action spectra) were calculated by measuring the photocurrent under monochromatic light at 0.2 V vs Ag/AgCl (~1.23 V vs RHE) according to the equation:

$$\mathrm{IPCE}(\%) = ([1240 \times J]/[\lambda \times P_{\mathrm{mono}}]) \times 100$$

where J is photocurrent density (mA cm^{-2}), λ is wavelength of incident light (nm), and P_{mono} is light power density (mW cm^{-2}). The IPCE value of TaON-treated electrode at 400 nm is ~5% as shown in Figure 6. It started to increase around 500 nm corresponding to the band gap energy of TaON. For TaON-as deposited/$CaFe_2O_4$ electrode, IPCE increased six times to ~30% at 400 nm. In previous reports about TaON electrodes,[12,13] IPCE of IrO_2-loaded TaON electrode presented a high value about 70%. But it comes from the effect of noble metal oxide co-catalyst, and there is no report about bare TaON electrode to compare. In this research, it is worth noting that the heterojunction formation with another metal oxide dramatically enhanced the efficiency without any co-catalyst.

It was expected that onset of IPCE would be ~600 nm like the absorption spectrum of $CaFe_2O_4$ (Figure 2b). But, the IPCE curve of the TaON-as deposited/$CaFe_2O_4$ electrode traced almost exactly the absorption curve of TaON instead of $CaFe_2O_4$. From the formation of TaON/$CaFe_2O_4$ heterojunction, we expected two effects from $CaFe_2O_4$ to help charge separation in the main absorber (TaON) to efficiently convert absorbed photons in TaON to current and to bring the additional light absorption especially from the long wavelength regions. Since the IPCE curve starts from 500 nm, one might think that only the first effect was realized and the increased IPCE is solely due to effective conversion of the light absorbed only by TaON. According to the band structure of $CaFe_2O_4$,[24] the direct transition (O^{2-} 2p → Fe^{3+} 4s, 3d) occurs under UV region (~350 nm, ~3.5 eV) and the indirect transition (Fe^{3+} d → d) is observed under visible light region (~620 nm, ~2 eV).[27,28] It was reported that the excited electrons and holes easily recombined when they were generated by the indirect transition.[27] In fact, if we expand the IPCE scale of TaON-as deposited/$CaFe_2O_4$ (Figure S8), small but significant IPCE values are observed in the 500−650 nm region. The IPCE of $CaFe_2O_4$ itself reported elsewhere[27] also started to increase around 500 nm in a very similar fashion as our TaON-as deposited/$CaFe_2O_4$. Thus the increased IPCE of TaON/$CaFe_2O_4$ below 500 nm could contain the contribution from photons absorbed by $CaFe_2O_4$ in addition to the improved conversion efficiency due to better charge separation. One might also suggest that the effect of $CaFe_2O_4$ may represent the role of an electrocatalyst of water oxidation. However, the onset of photocurrent did not shift toward negative potential, a typical response of an electrocatalyst of water oxidation (Figure S4b).

The working principle of this heterojunction photoanode system is illustrated in terms of energy diagram as presented in the Figure 7. When light is irradiated from back side of FTO, TaON absorbs the light and electrons, and holes are generated. $CaFe_2O_4$ absorbs the remaining light that also excites electrons

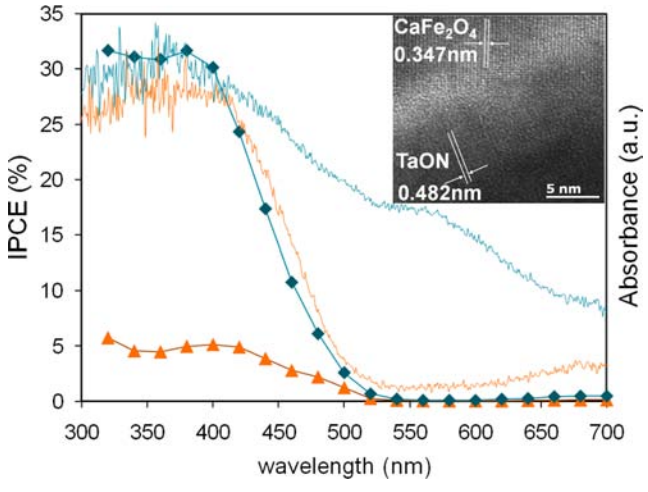

Figure 6. IPCE of TaON-treated electrode (triangle) and TaON-as deposited/$CaFe_2O_4$ electrode (diamond). IPCE was measured in 0.5 M NaOH at 0.2 V vs Ag/AgCl under monochromatic light irradiation. UV−vis DRS spectra of electrodes are also presented. The inset shows interface between TaON and $CaFe_2O_4$ layers.

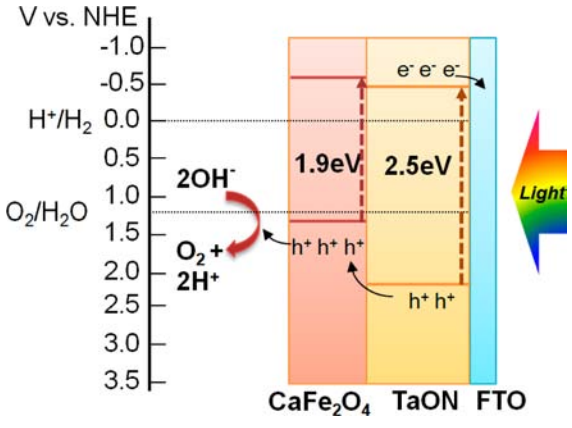

Figure 7. Energy diagram and expected charge flow of heterojunction photoanode. The conduction band and valence band of TaON and CaFe2O4 are presented with the redox potential of H^+/H_2 and O_2/H_2O.

dx.doi.org/10.1021/ja308723w | J. Am. Chem. Soc. 2013, 135, 5375−5383

and generates holes. The penetration of light all the way to $CaFe_2O_4$ was demonstrated experimentally as described in Figure S9. This junction structure brings more efficient utilization of incoming light than when only TaON is used for photoanode. Moreover, electrons from $CaFe_2O_4$ move toward FTO substrate through TaON, and holes from TaON migrate to surface of $CaFe_2O_4$ by using potential difference of the two semiconductors. Thus, $CaFe_2O_4$/TaON heterojunction photoanode can absorb more visible light, and the efficient charge separation across the junction structure improves its photoelectrochemical water oxidation activity. In the configuration shown in Figure 7, p-$CaFe_2O_4$ has to contact and oxidize water to generate O_2. But the downward band bending of p-type semiconductor is not beneficial for oxidation by holes. Putting n-TaON on the outer layer of the photoanode instead is, unfortunately, not possible because it cannot oxidize water due to mismatch of the band level between TaON and $CaFe_2O_4$. Thus although the current configuration is not an ideal way to take advantage of the p−n junction effect, we can still achieve charge separation by utilizing their staggered band configuration as shown.

To compare the present results with other reports in the literature, we measure the photocurrent density of TaON-as deposited/$CaFe_2O_4$ under more common conditions of the solar simulator (AM 1.5G, 100 mW cm^{-2}, model 91160, Oriel equipped with an air mass 1.5G filter) as shown in Figure S10. The solar to hydrogen efficiency was also calculated using following equation with assumption of 100% faradaic efficiency when the applied bias voltage was taken into account.

$$\eta_{STH} = I(\text{mA cm}^{-2}) \times (1.23\text{V} - V_{app})$$

The maximum η_{STH} obtained was 0.053% at 1 V (vs RHE). When the applied bias was not considered by assuming a tandem configuration of PEC cell with a PV device in the backside (V_{app} = 0), η_{STH} was 0.55% at 1.23 V (vs RHE).

Effects of Cocatalyst. Co-Pi has been extensively studied as a water oxidation co-catalyst for many semiconductor photocatalyst systems since its discovery.[40] This oxygen-evolving catalyst containing cobalt oxide and hydroxide species works well in a phosphate buffer solution.[41−43] Thus Co-Pi was introduced here to investigate its effect on the junction photoanode. Thus, Co-Pi was deposited on TaON electrode (TaON-treated) by applying 1 V vs Ag/AgCl for 2 min to form a thin catalyst layer. The success of deposition of Co-Pi was confirmed by XPS as shown in Figure S11.

The photocurrent density was measured in 0.1 M KPi buffered at pH 11.5 with 0.1 M KOH. Note that this electrolyte is optimized for Co-Pi and different from that used for Figures 4−6. First, Co-Pi deposition increased the photocurrent density of the TaON electrode more than three times (Figure 8a). Moreover, the onset potential of dark current clearly shifted to the lower value (1.3 V vs RHE). This dark current originates from Co-Pi deposited on the FTO substrate, because n-type semiconductors should not show anodic dark current. This indicates that Co-Pi acts as an effective electrocatalyst for water oxidation on the TaON photoanode. Then, Co-Pi was deposited on TaON (as-deposited)/$CaFe_2O_4$ junction electrode in the same way. When Co-Pi was deposited, the photocurrent increased by ∼70% for the junction photoanode as shown in Figure 8b. This is not a very significant increase relative to the TaON case. Instead, there was also a shift of onset potential of the dark current as in the TaON electrode.

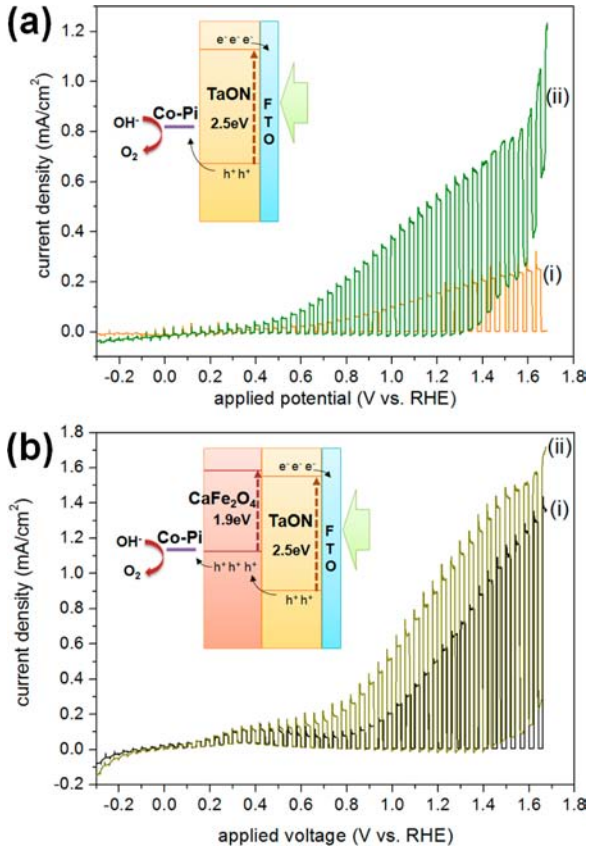

Figure 8. (a) Photocurrent density of (i) TaON-treated and (ii) TaON-treated/Co-Pi. (b) Photocurrent density of (i) TaON-as deposited/$CaFe_2O_4$ and (ii) TaON-as deposited/$CaFe_2O_4$/ Co-Pi in 0.1 M KPi solution buffered at pH 11.5 under visible light irradiation (λ > 420 nm). The schematic energy diagrams are also presented.

The catalytic mechanism of Co-Pi is not fully understood yet.[41] However, it is known that the photogenerated holes get involved in oxidizing cycle of Co-Pi.[42,44] The injected holes oxidize cobalt species from Co(II) to Co(III), Co(IV), and finally Co(IV)−O intermediates to yield oxygen as shown in the inset of Figure 8a for TaON.[42] Though the exact redox potential of these oxidation reactions is not revealed, a more positive valence band potential than the water oxidation potential is advantageous for photogenerated holes to be trapped by the catalytic cycle of Co-Pi and increases the efficiency of water oxidation.[45] As shown in the inset of Figure 8b, valence band of $CaFe_2O_4$ is already close to the water oxidation potential or the redox cycle of Co-Pi. Therefore the additional promoting effect of Co-Pi on TaON (as-deposited)/$CaFe_2O_4$ is marginal relative to the TaON electrode.

The evolution of hydrogen and oxygen gases during the photoelectrochemical water splitting reaction was measured for TaON-as deposited/$CaFe_2O_4$/Co-Pi electrode in 0.1 M KPi buffer solution of pH 11 in the three electrode system with an applied bias of 0.4 V vs Ag/AgCl (1.23 V vs RHE). The total amount of evolved hydrogen and oxygen was 123.38 and 58.72 μmol as shown in Figure 9. The stoichiometric ratio of H_2:O_2 evolved was 2.1:1. The slight excess of hydrogen appears to be due to the slow kinetics of oxygen evolution and self-oxidation of TaON as previously reported.[13,21]

The faradaic efficiency reached ∼80% for both hydrogen and oxygen evolution as shown in Table S1. The efficiency of oxygen evolution was <100%, probably due to the hole

dx.doi.org/10.1021/ja308723w | J. Am. Chem. Soc. 2013, 135, 5375−5383

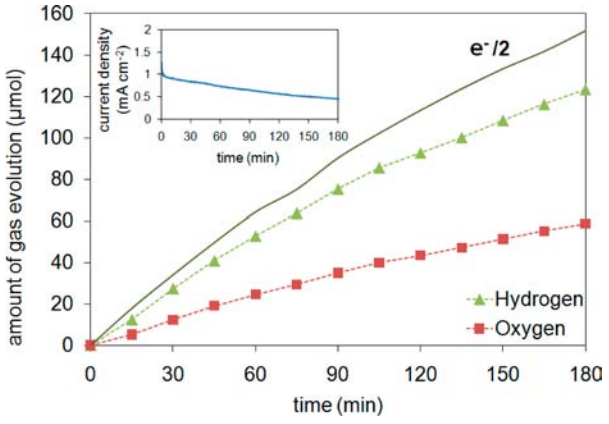

Figure 9. Hydrogen and oxygen evolution for TaON-as deposited/$CaFe_2O_4$/Co-Pi electrode in 0.1 M KPi buffer solution of pH 11 in three electrode system under visible light irradiation (λ > 400 nm). The applied bias was 0.4 V vs Ag/AgCl (1.23 V vs RHE). The expected amount of hydrogen molecules, $e^-/2$, is presented in a solid line. The inset shows time course of photocurrent generation.

consumption by self-oxidation of TaON especially during the initial period up to 1 h. In case of the hydrogen evolution the unwanted backward reaction between H_2 and O_2 could take place at the cathode and caused the efficiency decrease. In spite of those limitations, the results clearly show that this heterojunction photoanode can actually work for overall water splitting in photoelectrochemical cell. The stability of electrode was tested for 3 h (the current was measured simultaneously with the gas evolution as in the inset). The initial current, ~1 mA, decreased with time and reached about a half after 3 h. This does not represent a good stability and appears to be a characteristic of TaON because it is comparable to that of IrO_2-loaded TaON photoanode.[13] The beneficial role of co-catalyst was unequivocally revealed when we performed the same gas evolution experiments for TaON-as deposited/$CaFe_2O_4$ electrode without Co-Pi. As shown in Figure S12 and Table S2, the stability of current generation deteriorates, faradaic efficiency for hydrogen evolution decreases (50−70%), and the ratio of H_2:O_2 becomes significantly less than stoichiometric (1.5) without the co-catalyst. Thus, the oxygen-evolving catalyst, Co-Pi, is necessary to achieve stable and selective water splitting avoiding any parasitic processes.

CONCLUSIONS

A heterojunction photoanode was successfully fabricated between TaON and $CaFe_2O_4$ by electrophoretic deposition of two semiconductor powders. The photocurrent density derived from photoelectrochemical water oxidation under visible light increased five times relative to the single TaON electrode. The performance of the junction photoanode corresponded to ca. 30% of IPCE at λ < 400 nm, which is comparable to the state-of-the-art oxide photoanodes for PEC cells, especially without any co-catalyst. The introduction of $CaFe_2O_4$ brought the dramatic performance improvement by providing efficient charge separation across the formed junction structure and increasing the visible light absorption. The effect was revealed as greatly reduced resistance in the charge transfer across the electrode and electrolyte by electrochemical impedance spectroscopy analysis. The stoichiometric hydrogen and oxygen evolution was confirmed with the faradaic efficiency of ~80%.

ASSOCIATED CONTENT

Supporting Information

XRD pattern of TaON electrodes, optimization result of heterojunction, XPS analysis results, and additional photocurrent and IPCE. This material is available free of charge via the Internet at http://pubs.acs.org.

AUTHOR INFORMATION

Corresponding Author

jlee@postech.ac.kr

Notes

The authors declare no competing financial interest.

ACKNOWLEDGMENTS

This work was supported with the financial support by A3 Foresight program (NRF, Korea), Hydrogen Energy Centre (a Frontier Research Program of NRF, Korea), Artificial Photosynthesis (KCAP, NRF-2009-C1AAA001-2009-0093879), Basic Science Research Program (no. 2012-017247), Brain Korea 21 program and WCU program (R31-30005)

REFERENCES

(1) Fujishima, A.; Honda, K. *Nature* **1972**, *238*, 37−38.
(2) Sivula, K.; Le Formal, F.; Grätzel, M. *Chem. Sus. Chem* **2011**, *4*, 432−449.
(3) Jun, H.; Im, B.; Kim, J. Y.; Im, Y.-O.; Jang, J.-W.; Kim, E. S.; Kim, J. Y.; Kang, H. J.; Hong, S. J.; Lee, J. S. *Energy Environ. Sci.* **2012**, *5*, 6375−6382.
(4) Marsen, B.; Miller, E. L.; Paluselli, D.; Rocheleau, R. E. *Int. J. Hydrogen Energy* **2007**, *32*, 3110−3115.
(5) Hong, S. J.; Jun, H.; Borse, P. H.; Lee, J. S. *Int. J. Hydrogen Energy* **2009**, *34*, 3234−3242.
(6) Ng, Y. H.; Iwase, A.; Kudo, A.; Amal, R. *J. Phys. Chem. Lett.* **2010**, *1*, 2607−2612.
(7) Iwase, A.; Kudo, A. *J. Mater. Chem.* **2010**, *20*, 7536.
(8) Hong, S. J.; Lee, S.; Jang, J. S.; Lee, J. S. *Energy Environ. Sci.* **2011**, *4*, 1781−1787.
(9) Maeda, K.; Teramura, K.; Lu, D.; Takata, T.; Saito, N.; Inoue, Y.; Domen, K. *Nature* **2006**, *440*, 295−295.
(10) Tang, J.; Zou, Z.; Ye, J. *J. Phys. Chem. B* **2003**, *107*, 14265−14269.
(11) Kim, H. G.; Borse, P. H.; Jang, J. S.; Ahn, C. W.; Jeong, E. D.; Lee, J. S. *Adv. Mater.* **2011**, *23*, 2088−92.
(12) Abe, R.; Higashi, M.; Domen, K. *J. Am. Chem. Soc.* **2010**, *132*, 11828−11829.
(13) Higashi, M.; Domen, K.; Abe, R. *Energy Environ. Sci.* **2011**, *4*, 4138−4147.
(14) Nishimura, N.; Raphael, B.; Maeda, K.; Le Gendre, L.; Abe, R.; Kubota, J.; Domen, K. *Thin Solid Films* **2010**, *518*, 5855−5859.
(15) Ishikawa, A.; Takata, T.; Kondo, J. N.; Hara, M.; Domen, K. *J. Phys. Chem. B* **2004**, *108*, 11049−11053.
(16) Yokoyama, D.; Hashiguchi, H.; Maeda, K.; Minegishi, T.; Takata, T.; Abe, R.; Kubota, J.; Domen, K. *Thin Solid Films* **2011**, *519*, 2087−2092.
(17) Pendlebury, S. R.; Cowan, A. J.; Barroso, M.; Sivula, K.; Ye, J.; Gratzel, M.; Klug, D. R.; Tang, J.; Durrant, J. R. *Energy Environ. Sci.* **2012**, *5*, 6304−6312.
(18) Su, J.; Guo, L.; Bao, N.; Grimes, C. A. *Nano Lett.* **2011**, *11*, 1928−1933.
(19) McDonald, K. J.; Choi, K.-S. *Chem. Mater.* **2011**, *23*, 4863−4869.
(20) Hitoki, G.; Takata, T.; Kondo, J. N.; Hara, M.; Kobayashi, H.; Domen, K. *Chem. Commun.* **2002**, *16*, 1698−1699.
(21) Takata, T.; Hitoki, G.; Kondo, J.; Hara, M.; Kobayashi, H.; Domen, K. *Res. Chem. Intermed.* **2007**, *33*, 13−25.

(22) Kim, H. G.; Borse, P. H.; Choi, W.; Lee, J. S. *Angew. Chem., Int. Ed.* **2005**, *44*, 4585−4589.
(23) Kim, H. G.; Borse, P. H.; Jang, J. S.; Jeong, E. D.; Jung, O. S.; Suh, Y. J.; Lee, J. S. *Chem. Commun.* **2009**, *39*, 5889−5891.
(24) Matsumoto, Y. *J. Solid. State. Chem.* **1996**, *126*, 227−234.
(25) Chun, W.-J.; Ishikawa, A.; Fujisawa, H.; Takata, T.; Kondo, J. N.; Hara, M.; Kawai, M.; Matsumoto, Y.; Domen, K. *J. Phys. Chem. B* **2003**, *107*, 1798−1803.
(26) Fornarini, L.; Nozik, A. J.; Parkinson, B. A. *J. Phys. Chem.* **1984**, *88*, 3238−3243.
(27) Ida, S.; Yamada, K.; Matsunaga, T.; Hagiwara, H.; Matsumoto, Y.; Ishihara, T. *J. Am. Chem. Soc.* **2010**, *132*, 17343−17345.
(28) Cao, J.; Kako, T.; Li, P.; Ouyang, S.; Ye, J. *Electrochem. Commun.* **2011**, *13*, 275−278.
(29) El Sherif, M.; Bayoumi, O. A.; Sokkar, T. Z. N. *Color Res. Appl.* **1997**, *22*, 32−39.
(30) Ji, S. M.; Choi, S. H.; Jang, J. S.; Kim, E. S.; Lee, J. S. *J. Phys. Chem. C* **2009**, *113*, 17824−17830.
(31) Barroso, M.; Cowan, A. J.; Pendlebury, S. R.; Grätzel, M.; Klug, D. R.; Durrant, J. R. *J. Am. Chem. Soc.* **2011**, *133*, 14868−14871.
(32) Armytage, D.; Fender, B. E. F. *Acta Crystallogr., Sect. B* **1974**, *30*, 809−812.
(33) Decker, B. F.; Kasper, J. S. *Acta Crystallogr.* **1957**, *10*, 332−337.
(34) Fan, G.; Gu, Z.; Yang, L.; Li, F. *Chem. Eng. J.* **2009**, *155*, 534−541.
(35) Khoo, E.; Lee, P. S.; Ma, J. *J. Eur. Ceram. Soc.* **2010**, *30*, 1139−1144.
(36) Ng, S. Y.; Boccaccini, A. R. *Mater. Sci. Eng., B* **2005**, *116*, 208−214.
(37) Sarkar, P.; Nicholson, P. S. *J. Am. Chem. Soc.* **1996**, *79*, 1987−2002.
(38) Xie, Y.; Zhou, L.; Lu, J. *J. Mater. Sci.* **2009**, *44*, 2907−2915.
(39) Kim, J. Y.; Jun, H.; Hong, S. J.; Kim, H. G.; Lee, J. S. *Int. J. Hydrogen Energy* **2011**, *36*, 9462−9468.
(40) Kanan, M. W.; Nocera, D. G. *Science* **2008**, *321*, 1072−5.
(41) Steinmiller, E. M.; Choi, K. S. *Proc. Natl. Acad. Sci. U.S.A.* **2009**, *106*, 20633−6.
(42) Zhong, D. K.; Gamelin, D. R. *J. Am. Chem. Soc.* **2010**, *132*, 4202−4207.
(43) Young, E. R.; Costi, R.; Paydavosi, S.; Nocera, D. G.; Bulovic, V. *Energy. Environ. Sci.* **2011**, *4*, 2058−2061.
(44) Pijpers, J. J. H.; Winkler, M. T.; Surendranath, Y.; Buonassisi, T.; Nocera, D. G. *Proc. Natl. Acad. Sci. U.S.A.* **2011**, *108*, 10056−10061.
(45) Zhong, D. K.; Sun, J.; Inumaru, H.; Gamelin, D. R. *J. Am. Chem. Soc.* **2009**, *131*, 6086−6087.